Possible origin of β-relaxation in amorphous metal alloys from atomic-mass differences of the constituents

Bingyu Cui,[1] Zach Evenson,[2] Beibei Fan,[3] Mao-Zhi Li,[3] Wei-Hua Wang,[4,*] and Alessio Zaccone[1,5,†]

[1]*Statistical Physics Group, Department of Chemical Engineering and Biotechnology, University of Cambridge, Philippa Fawcett Drive, CB3 0AS Cambridge, United Kingdom*

[2]*Heinz Maier-Leibnitz Zentrum and Physik Department, Technische Universität München, Lichtenbergstrasse 1, 85748 Garching, Germany*

[3]*Department of Physics, Renmin University of China, Beijing 100872, China*

[4]*Institute of Physics, Chinese Academy of Sciences, Beijing 100190, China*

[5]*Cavendish Laboratory, University of Cambridge, JJ Thomson Avenue, CB3 0HE Cambridge, United Kingdom*

(Received 23 June 2018; published 4 October 2018)

We employ an atomic-scale theory within the framework of nonaffine lattice dynamics to uncover the origin of the Johari-Goldstein (JG) β-relaxation in metallic glasses (MGs). Combining simulation and experimental data with our theoretical approach, we reveal that the large mass asymmetry between the elements in a $La_{60}Ni_{15}Al_{25}$ MG leads to a clear separation in the respective relaxation timescales, giving strong evidence that JG relaxation is controlled by the lightest atomic species present. Moreover, we show that only qualitative features of the vibrational density of states determine the overall observed mechanical response of the glass, paving the way for a possible unified theory of secondary relaxations in glasses.

DOI: 10.1103/PhysRevB.98.144201

I. INTRODUCTION

The diversity of atomic motion in metallic glasses (MGs) is central to their unique physical and mechanical properties. The primary or α-relaxation underlies the drastic slowing down of the collective atomic dynamics during the transition from a viscous supercooled liquid to a glassy solid upon cooling, and its origin is still an outstanding problem in condensed-matter physics. Indeed, like many other disordered solids, such as polymers and molecular glasses, MGs exhibit an entire class of secondary relaxations that persist even well below the glass transition temperature T_g [1–3]. These phenomena are broadly referred to as β-relaxations and occur on timescales much shorter than that of the α-relaxation. The Johari-Goldstein (JG) β-relaxation is the most well known among these due to its ubiquity in all types of glasses [4,5]. Although the exact atomic-scale mechanism underlying the JG β-relaxation in MGs is still not clear, there appears to be a correlation to the α-relaxation, deformation, and mechanical properties (see [1] and references therein). In this regard, unraveling the atomic-scale dynamical features of the JG β-relaxation would represent considerable progress in our current understanding of its microscopic origin and its impact on the physical and materials properties of glasses [6].

A key open question is about the role of different atomic/molecular constituents in the various relaxation processes, and in particular whether a relaxation process is controlled by the dynamics of a particular type of constituent(s). In the case of organic molecular glasses it has been recently argued that all molecules seem to participate in the JG relaxation, although not all at once [7]. This problem has not been investigated in metallic glasses, although the relative contributions of different atomic species to the peak temperature of the JG relaxation has been addressed in [8].

While many studies have examined both the structural and relaxational features of the JG β-relaxation in MGs [9–12] the connection to the atomic-scale vibrational properties remains, to date, greatly unexplored. The JG β-relaxation in MGs generally occurs on microsecond timescales, some several orders of magnitude smaller than the α-relaxation of the glass [10,13]. However, accessing the atomic-scale dynamics of MGs in this temporal regime is both experimentally and computationally challenging. Novel coherent x-ray scattering techniques probe collective atomic motion on timescales larger than about 1 s [11,14], while molecular dynamics (MD) simulations of the MG glassy-state dynamics have been only recently successfully tested up to 10 ms [10].

Here, we combine experimental and simulation investigations with a microscopic theoretical framework of viscoelastic response and relaxation of MGs. With this approach, we are able to unveil the atomic-scale dynamics in MGs on timescales over some 12 orders of magnitude, thus providing necessary, complementary information for advanced simulation and experimental studies.

Considering the success of our recent theoretical work in linking the low-energy boson peak (BP) with α-relaxation and dynamical heterogeneity in glasses [15,16], the results presented in this paper give insight into the atomic-scale dynamical facets of the JG β-relaxation in MGs. In particular, we are able to show strong evidence that the JG β-relaxation is controlled by the smallest (lightest) atomic-scale species present in the MG and that the existence of two relaxation modes (α and JG β) can be traced down to the large

*whw@iphy.ac.cn
†az302@cam.ac.uk

 ©2018 American Physical Society

differences in atomic mass of the metallic elements that comprise the MG.

II. EXPERIMENTAL METHODS

A. Dynamical mechanical analysis

The dynamical mechanical analysis experiments were carried out according to the procedure outlined in Ref. [8] using a TAQ800 dynamical mechanical analyzer. Fully amorphous cylindrical samples of $La_{60}Ni_{15}Al_{25}$ with a diameter of 2 mm were tested using the single-cantilever bending method in an isothermal mode with a strain amplitude of 5 μm, temperature step of 3 K, and discrete testing frequencies of 1, 2, 4, 8, and 16 Hz. The complex viscoelastic shear modulus is obtained as $G(\omega, T) = G'(\omega, T) + iG''(\omega, T)$ as a function of test frequency ω and temperature T, with mechanical relaxations appearing as peaks in the loss modulus $G''(\omega, T)$.

B. Inelastic neutron scattering

Glassy ribbons of $La_{60}Ni_{15}Al_{25}$ were produced by melt spinning at the Institute for Physics, Chinese Academy of Sciences, in Beijing. About 12 m of ribbons with a cross section of 2.5×0.06 mm^2 were placed in a thin-walled aluminum hollow cylinder (height 51 mm, diameter 20 mm, thickness 0.55 mm) for the inelastic neutron scattering (INS) experiments at the time-of-flight spectrometer TOFTOF in Garching. An incident wavelength of $\lambda_i = 2.8$ Å resulted in an accessible momentum transfer range of $0.8 \leqslant q \leqslant 4.2$ Å^{-1} at zero-energy transfer. The raw data were normalized to a vanadium standard, corrected for empty container scattering and sample shelf absorption, and interpolated to constant q in order to obtain the dynamic structure factor. The background was corrected by separate measurements of the cryostat with an empty sample holder. As the scattering probability of the ribbons was calculated to be around 8%, multiple-scattering effects were neglected.

In order to access the largest energy transfer range available, only the data located on the neutron energy gain side of the spectrometer were analyzed. In a multicomponent system with predominantly coherent scatterers, a generalized, neutron-weighted vibrational density of states (VDOS) $D(\omega_p)$ can be obtained under the incoherent one-phonon approximation, where the measured dynamic structure factor, integrated over the accessible q range, is proportional to $D(\omega_p)/\omega_p^2$ [17]. The neutron-weighted VDOS was obtained in an iterative procedure using the FRIDA-1 software [18,19].

III. MOLECULAR DYNAMICS SIMULATIONS

Classical MD simulations were performed for the $La_{60}Ni_{15}Al_{25}$ metallic alloy system using the LAMMPS package [20]. The interatomic interactions were described by the embedded-atom method potential in Ref. [21]. Details can be found in the Appendix. To obtain the VDOS $D(\omega_p)$ of the system at various temperatures, the direct diagonalization method was adopted, in which the steepest-descent method is carried out for the final configuration.

The structure model contains 10 000 atoms in a cubic box with periodic boundary conditions applied in three dimensions. It was first fully equilibrated at $T = 2000$ K for 1 ns in the NPT (isobaric and isothermal) ensemble, then cooled down to 300 K with a cooling rate of 10^{12} K/s. In the cooling process, the box size was adjusted to give zero pressure. At 300 K, the structure was then relaxed for 2 ns in the NPT ensemble. To obtain the atomic structures at 330, 360, 390, and 410 K, the structure at 300 K was then heated with a heating rate of 10^{10} K/s and then relaxed for 2 ns in the NPT ensemble at each temperature of interest. The MD step was set to be 2 fs.

The dynamical matrix corresponding to the potential-energy minimum reached by LAMMPS line search algorithm minimization is given by

$$H_{ij} = \frac{1}{\sqrt{m_i m_j}} \frac{\partial^2 U}{\partial \underline{x}_i \partial \underline{x}_j}, \tag{1}$$

where U is the total internal energy of the system (which is a function of all atoms' coordinates), m_i is the mass of atom i, and $\underline{x}_i$ is the coordinate vector of atom i. The VDOS can be calculated by directly diagonalizing the dynamical matrix as

$$D(\omega_p) = \frac{1}{3N-3} \sum_{\lambda} \delta(\omega_p - \omega_\lambda), \tag{2}$$

where ω_λ is the eigenfrequency.

IV. NONAFFINE LATTICE DYNAMICS

A. From the generalized Langevin equation to the dynamic viscoelastic moduli

The dynamics of atoms in disordered solids is typically nonaffine, which means that the atoms in the deformed configuration do not sit in the positions prescribed by the strain tensor; that is, they do not get displaced according to an affine transformation. The latter would give the new position of the atom from the left multiplication of the strain tensor and position vector of the atom at rest. Instead, in disordered systems, the atom in the affine position receives forces from the nearest neighbors which do not balance (they would balance and cancel to zero in a centrosymmetric crystal, owing to local inversion symmetry of the lattice). Hence, the lattice dynamics for amorphous materials has to be rewritten to take these facts into account [22], which eventually leads to softening of the elastic constants [23] and new physics which is currently being explored.

Upon applying a deformation described by the strain tensor $\underline{\underline{\eta}}$, the dynamics of a tagged particle i interacting with other atoms in the reference frame satisfies the following equation for the (mass-scaled) displacement $\{\underline{x}_i(t) = \mathring{\underline{q}}_i(t) - \mathring{\underline{q}}_i\}$ around a known rest frame $\mathring{\underline{q}}_i$ (see Ref. [15] for derivation):

$$\frac{d^2 \underline{x}_i}{dt^2} + \int_{-\infty}^{t} \nu_i(t-t') \frac{d\underline{x}_i}{dt'} dt' + \sum_j \underline{\underline{H}}_{ij} \underline{x}_j = \underline{\Xi}_{i,xy} \eta_{xy}. \tag{3}$$

Note that the summation convention over repeated indices is not used. This equation can be solved by performing Fourier transformation followed by normal-mode decomposition that decomposes the $3N$-vector $\underline{\tilde{x}}$ (which contains positions of all atoms) into normal modes $\underline{\tilde{x}} = \hat{\tilde{x}}_p(\omega) \underline{\phi}_p$ (p is the index

labeling the normal modes). Note that we focus on time-dependent shear strain $\eta_{xy}(t)$. For this case, the vector $\underline{\Xi}_{i,xy}$ represents the force per unit strain acting on atom i due to the motion of its nearest neighbors (see, e.g., [22] for a more detailed discussion).

As shown in the Appendix, Eq. (3) can be manipulated into the following form:

$$-\omega^2(\underline{\underline{\Phi}}^T\cdot\underline{\tilde{x}})+i\omega\underline{\underline{\Phi}}^T\underline{\underline{\tilde{\nu}}}(\omega)\underline{\underline{\Phi}}\underline{\underline{\Phi}}^T\cdot\underline{\tilde{x}}+\underline{\underline{D}}\,(\underline{\underline{\Phi}}^T\cdot\underline{\tilde{x}}) = \underline{\underline{\Phi}}^T\cdot\underline{\Xi}_{xy}\tilde{\eta}_{xy}, \tag{4}$$

where the matrix $\underline{\underline{\Phi}}$ consists of the $3N$ eigenvectors $\underline{\phi}_p$ of the Hessian. Here, we have $(\underline{\underline{\Phi}}^T\underline{\underline{\tilde{\nu}}}\underline{\underline{\Phi}})_{mn}=\sum_i\Phi_{im}\Phi_{in}\tilde{\nu}_i$ and $(\Phi^T\Phi)_{mn}=\sum_i\Phi_{im}\Phi_{in}=\delta_{mn}$, where $\underline{\underline{\tilde{\nu}}}$ is the diagonal matrix made by $\tilde{\nu}_i(\omega)$ along the diagonal. For different tagged particles i and in general, one cannot find a solution without simplifying the term $\underline{\underline{\Phi}}^T\underline{\underline{\nu}}\underline{\underline{\Phi}}$, which establishes coupling between different eigenmode contributions to the friction.

The friction term coupled to the pth normal mode is thus $i\omega\sum_{im}\Phi_{im}\Phi_{ip}\tilde{\nu}_i$. At this point of the analysis, we need to work with the assumption that $\underline{\underline{\Phi}}^T\underline{\underline{\nu}}\underline{\underline{\Phi}}$ is a diagonal matrix. In physical terms, this means that the damping is not correlated across different eigenmodes. This is an approximation used within this framework to make the model solvable [15]. Thus, the friction that the pth mode feels is dominated by $i\omega\sum_i(\Phi_{ip})^2\tilde{\nu}_i$. This result is used in the section below to justify the form of the memory kernel for the friction coefficient based on differences in atomic mass of the constituents.

As derived in our previous work [15], we use the generalized Langevin equation (3) under normal-mode decomposition while accounting for nonaffine displacements to derive a microscopic expression for the complex viscoelastic modulus

$$G^*(\omega)=G_A-3\rho\int_0^{\omega_D}\frac{D(\omega_p)\Gamma(\omega_p)}{\omega_p^2-\omega^2+i\tilde{\nu}(\omega)\omega}d\omega_p, \tag{5}$$

where we have dropped the Cartesian indices for convenience and $\rho=N/V$ denotes the atomic density of the solid. $\Gamma(\omega_p)$ is a function which describes the correlation of nonaffine forces in the frequency shell [22–24].

B. Qualitative arguments for the form of the friction kernel in $La_{60}Ni_{15}Al_{25}$

As has been shown above in the context of Eq. (4), the friction that the pth mode feels is given by $\sum_i(\Phi_{ip})^2\nu_i$. We expand this term explicitly in terms of the different atomic species which form the alloy:

$$\begin{aligned}\sum_i(\Phi_{ip})^2\nu_i &\sim \sum_{Al}^{25}\left(\Phi_{ip}^2\right)\sum_\alpha\frac{m_\alpha}{m_{Al}}\frac{c_{\alpha,Al}^2}{\omega_\alpha^2}\cos(\omega_\alpha t)\\ &+\sum_{La}^{60}\left(\Phi_{ip}^2\right)\sum_\alpha\frac{m_\alpha}{m_{La}}\frac{c_{\alpha,La}^2}{\omega_\alpha^2}\cos(\omega_\alpha t)\\ &+\sum_{Ni}^{15}\left(\Phi_{ip}^2\right)\sum_\alpha\frac{m_\alpha}{m_{Ni}}\frac{c_{\alpha,Ni}^2}{\omega_\alpha^2}\cos(\omega_\alpha t)\end{aligned}$$

$$\begin{aligned}&=\sum_\alpha\sum_{Al}^{25}(\Phi_{ip})^2\frac{m_\alpha}{m_{Al}}\frac{c_{\alpha,Al}^2}{\omega_\alpha^2}\cos(\omega_\alpha t)\\ &+\sum_\alpha\sum_{La}^{60}(\Phi_{ip})^2\frac{m_\alpha}{m_{La}}\frac{c_{\alpha,La}^2}{\omega_\alpha^2}\cos(\omega_\alpha t)\\ &+\sum_\alpha\sum_{Ni}^{15}(\Phi_{ip})^2\frac{m_\alpha}{m_{Ni}}\frac{c_{\alpha,Ni}^2}{\omega_\alpha^2}\cos(\omega_\alpha t).\end{aligned} \tag{6}$$

The role of Φ_{ip} here is to give a weight to each ν_i contribution in the sum. All these sums could also be written as integrals upon replacing the discrete variable ω_α with the continuous eigenfrequency ω_p and introducing the VDOS as a factor in the integral over ω_p. Here, one can find that each term is inversely proportional to the mass of the atomic species in question. We note that the atomic mass of La (138.9 u) is more than two times as large as the mass of Ni (58.7 u) and five times larger than the mass of Al (26.98 u), which gives a much larger weight in the sum of the Al and Ni terms. Hence, taking also stoichiometry into account, the two terms relative to Ni and Al considered together are about three times larger than the contribution of the La term.

In order to strengthen this claim, we also consider the role of the unknown dynamical coupling coefficients c_α which appear in Eq. (6). While the values of these coefficients cannot be determined from first principles, we can still obtain valuable indications about the probable magnitude by considering quantities like the partial $g(r)$ functions in the system. Since these coefficients are associated with medium-range (or, generically, beyond-short-range) dynamics, features in $g(r)$ may give an indication of the relative magnitude of the dynamical coupling between different species in the alloy.

Also, while $g(r)$ is a static structural quantity, it is also true that it is directly related to dynamics via the Boltzmann inversion relation, which yields the potential of mean force as $V_{mfp}/k_BT=-\ln g(r)$. In turn, the potential of the mean force represents the interaction energy between two atoms mediated by the presence of all other atoms in the system; hence, it also contains many-body effects. Therefore, $g(r)$ is directly related to the potential of the mean force, which in turn influences the correlated motions (hence the dynamics) of the atoms and establishes (e.g., through long-range attractions) the dynamic coupling.

Consideration of the pair correlation function obtained from simulations and shown in Fig. 1 indicates that there is a clear broad peak for Al-Al in the regime of the medium-range order. This supports our claim that the JG β-relaxation is due to medium-range correlations and coupling between Al atoms. This broad peak of Al-Al with respect to the short-range order peak stands out in comparison with the other contributions in the medium-range regime.

Finally, not only will the prefactor of the memory function of La be smaller than the other two atomic species for the reason above, but also the characteristic timescale of the memory decay associated with La will be comparatively larger, as the relaxation time is typically inversely proportional to the mass (or at least inversely proportional to the square root of the mass). Hence, the contribution of La to memory and hence to the intermediate-scattering function (ISF) would be at a somewhat longer timescale compared to Ni. Additionally,

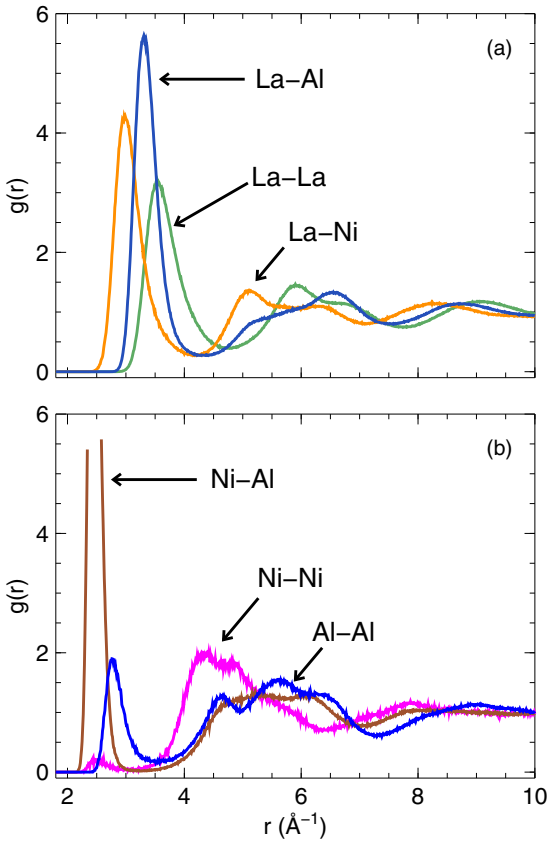

FIG. 1. Partial contributions to the radial distribution function $g(r)$ as calculated from MD simulations for $La_{60}Ni_{15}Al_{25}$ at $T = 300$ K. The large maximum of the Ni-Al partial in (b) occurs at $g(r_{max}) = 12$, which falls out of the range of the vertical axis of the plot.

this contribution would probably be hybridized or obscured by Ni, which has a larger prefactor and would explain why we result in only two decays in our model for the ISF and memory function.

These arguments, which indicate that the La term in the form of the memory function given by Eq. (6) may be negligible, can be summarized as follows: (i) the mass factor in the denominator makes the contribution of La about three times smaller than the two contributions of Ni and Al taken together. (ii) The main medium-range contributions to the features of $g(r)$ emanate from Al, which corroborates the hypothesis that the c_α coefficients are larger for Al and justify the dominance of Al dynamics in the JG β-relaxation. (iii) If modeled as a third stretched-exponential function, the contribution of La would have a larger characteristic timescale of decay and would show up at longer times, probably masked or hybridized with the Ni contribution. Based on this approximation, the form of the memory function for the interatomic friction in Eq. (6) reduces to

$$\nu(t) = \sum_{\alpha}\sum_{Ni}^{15}(\Phi_{ip})^2\frac{m_\alpha}{m_{Ni}}\frac{c_{\alpha,Ni}^2}{\omega_\alpha^2}\cos(\omega_\alpha t) + \sum_{\alpha}\sum_{Al}^{25}(\Phi_{ip})^2\frac{m_\alpha}{m_{Al}}\frac{c_{\alpha,Al}^2}{\omega_\alpha^2}\cos(\omega_\alpha t) = \nu_1(t)+\nu_2(t), \tag{7}$$

where $\nu_1(t)$ and $\nu_2(t)$ are two generic functions of time that will be specified in the next section.

V. RELATION BETWEEN FRICTION MEMORY KERNEL AND INTERMEDIATE-SCATTERING FUNCTION

For a supercooled liquid, a relationship between the time-dependent friction, which is dominated by slow collective dynamics, and the intermediate-scattering function was famously derived within kinetic theory by Sjoegren and Sjoelander [25] (see also Ref. [26]):

$$\nu(t) = \frac{\rho k_B T}{6\pi^2 m}\int_0^\infty dq q^4 F_s(q,t)c(q)^2F(q,t), \tag{8}$$

where m is a characteristic mass, $c(q)$ is the direct correlation function of liquid-state theory, $F(q,t)$ is the intermediate-scattering function, and $F_s(q,t)$ is the self-part of $F(q,t)$ [25]. All of these quantities are functions of the wave vector q, and the integral over q leaves a time dependence of $\nu(t)$, which is exclusively given by the product $F_s(q,t)F(q,t)$. Upon further approximating $F_s(q,t)F(q,t) \sim F(q,t)^2$, we obtain an intermediate-scattering function via

$$F(q,t) \sim \sqrt{\nu(t)}. \tag{9}$$

That the VDOS is related to $\nu(t)$ becomes evident upon considering the following relation, which holds for the particle-bath Hamiltonian from which Eq. (3) is derived [15,16,27],

$$\nu(t) = \int_0^\infty d\omega_p D(\omega_p)\frac{\gamma(\omega_p)^2}{\omega_p^2}\cos\omega_p t,$$

which couples the dynamics of the tagged atom to that of all the oscillators forming the bath, which represent all the other atomic degrees of freedom in the material.

VI. RESULTS AND DISCUSSION

A. Radial distribution function and partials thereof

From the MD simulations we obtain the partial pair correlation functions $g(r)$ for all atomic pairs and show them in Fig. 1. The partial functions shown in Fig. 1(b) clearly indicate that, in the regime of the medium-range order (between $r = 4$ Å and $r = 7$ Å), there are broad peaks for Ni-Ni and Al-Al which are either much larger or comparable in magnitude to the primary peak associated with the short-range order (up to $r \sim 3$ Å). In contrast to the La pairs, in which the short-range-order peak appears to be the most dominant [Fig. 1(a)], the more active Ni-Ni and Al-Al pair interactions at the length scale of the medium-range order would also indicate a stronger dynamical coupling in this spatial regime.

B. Vibrational density of states

The solid gray circles in Fig. 2 represent the total $D(\omega_p)$ as obtained from MD simulations. A more detailed look at the VDOS can be seen through the respective contributions of the La, Ni, and Al atoms. It is clear that the initial maximum of the total $D(\omega_p)$ at around 8 meV is attributed to low-energy

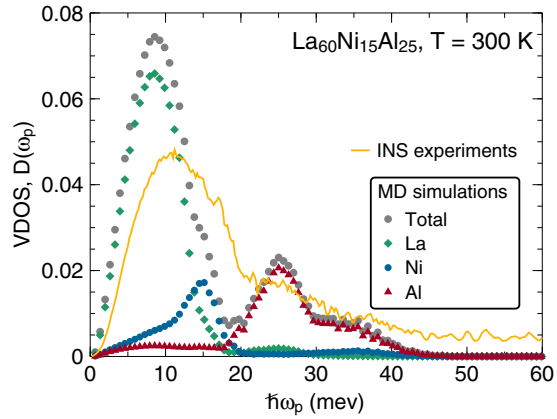

FIG. 2. Vibrational density of states (VDOS) of $La_{60}Ni_{15}Al_{25}$ at $T = 300$ K as determined in INS experiments (solid line) and MD simulations (symbols).

vibrations involving the heavy La atoms, while vibrations of the Ni atoms occur around 15 meV and are responsible for an apparent shoulder on the high-energy side of the main vibrational band. The vibrational dynamics of the light Al atoms are, in contrast, well separated from that of the other elements and exhibit a double-band structure at around 25 and 35 meV. $D(\omega_p)$ as obtained in INS experiments is shown alongside the simulation data. It is important to note here that the experimental $D(\omega_p)$ is additionally weighted by the isotope-specific neutron scattering cross sections of the constituent elements, of which Ni-Ni and Ni-La atomic pairs will dominate. Hence, the experimental $D(\omega_p)$ should be taken to represent only a generalized, neutron-weighted VDOS. In any case, it is apparent that the predominant contribution to the high-frequency side of both VDOSs of this MG stems from the vibrations of the Al atoms.

C. Dynamic mechanical analysis and comparison with theory

In Fig. 3 we show a master curve of the experimentally measured $G''(\omega)$ obtained from Ref. [8] for $La_{60}Ni_{15}Al_{25}$ at a reference temperature of 453 K, together with a theoretical fitting provided by Eq. (5). The α-relaxation appears as the

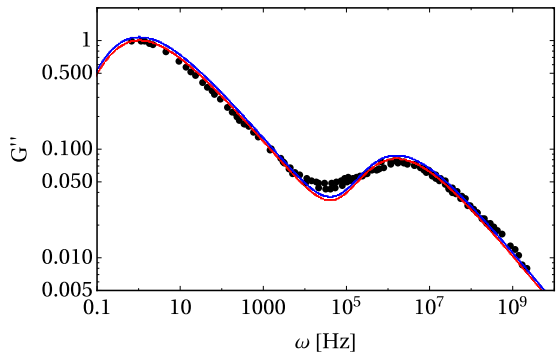

FIG. 3. Master curve of the imaginary part of the complex viscoelastic modulus $G''(\omega)$ at a reference temperature $T = 453$ K. The red and blue curves are fit results to our theoretical model using the experimental and simulated VDOSs, respectively, as input.

main loss peak situated around 1 Hz. A distinct feature of this system is the prominent and well-separated loss peak on the high-frequency side around 10^6 Hz and is attributed to the JG β-relaxation.

The nonaffine lattice dynamic theory of viscoelasticity of glasses outlined above allows us to quantitatively link the macroscopic features of the JG β-relaxation with the atomic-scale vibrational properties of this MG. Within this framework, it is possible to rationalize the average friction in the atomic motion of a tagged atom in the glass in terms of the respective contributions of the atomic components, for which the friction coefficient of the ith atom ν_i is proportional to the reciprocal of the atomic mass of atom i [15,27]. Thus, as was shown in Sec. IV B, when summing over all tagged atoms in $i\omega\sum_i(\Phi_{ip})^2\tilde{\nu}_i$, the contributions to the friction coefficient coming from the heaviest atoms, i.e., La, turn out to be smaller by at least a factor of $1/3$ in comparison with the contributions of Al and Ni (taken together). For the case of $La_{60}Ni_{15}Al_{25}$ we thus find that the contribution of La can be neglected, given the comparatively very large mass of La, which leaves the average friction as the sum of two contributions, those of Ni and Al, which carry widely different relaxation timescales by virtue of the different atomic masses.

As derived in Sec. IV B, in the sum over i only terms corresponding to Ni and Al atoms survive, which are well separated in magnitude given the difference in mass between Ni and Al. We then divide the sum into two groups for Ni and Al and then average each group separately. The final result is that the average friction memory function consists of two distinct contributions, according to Eq. (7), both of which will decay in time but with two different and well-separated relaxation times, τ_1 and τ_2. The shorter relaxation time τ_2 (associated with the JG β-relaxation) is related to the atomic dynamics of the lighter element, Al, whereas the other term has a longer relaxation time τ_1, dominated by the atomic dynamics of the heavier element, Ni, which contributes to the α-relaxation time.

With an appropriate ansatz for $\nu(t)$ we obtain the intermediate-scattering function $F(q,t)$ via $\nu(t) \sim F(q,t)^2$ [25,26]. From experiments and simulations, we know that in supercooled liquids $F(q,t) \sim \exp[(-t/\tau)^b]$ for the α-relaxation, where τ is the characteristic structural relaxation time and b is the stretching exponent with values normally between $b = 0.5$ and 0.7 [28]. When both α- and β-relaxations are present, $F(q,t)$ has a two-step decay, with the first decay at shorter times due to the β-relaxation and the second decay at much longer times due to the α-relaxation. On the basis of this evidence, we take the time dependence of each of the two terms in the memory function to be stretched exponential with different values of τ and b,

$$\nu(t) \sim \exp[-(t/\tau_1)^{b_1}] + c\exp[-(t/\tau_2)^{b_2}], \qquad (10)$$

where c is a constant.

The curves in Fig. 3 are our fits to experimental data using the VDOS obtained in both INS experiments (red) and MD simulations (blue). It is apparent that our theoretical model excellently captures both peaks in the loss spectrum over a frequency range of some ten orders of magnitude with the resulting parameters: $\tau_1 = 0.67$ s, $b_1 = 0.45$, $\tau_2 = 4.04 \times 10^{-7}$ s, $b_2 = 0.47$, and $c = 0.07$. We note here that the two-

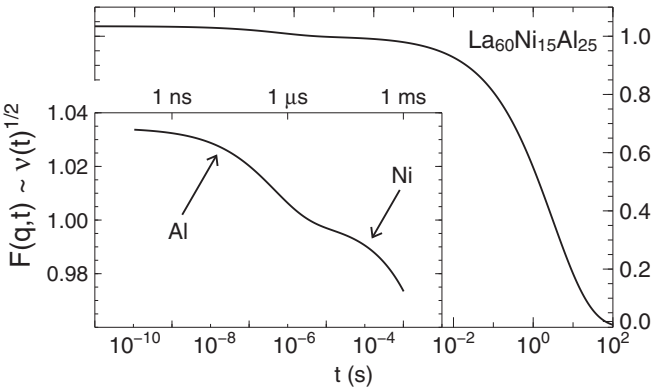

FIG. 4. Time decay of the square root of the total memory function for the friction $\nu(t)$, exhibiting two decays corresponding to α and β decay in the intermediate-scattering function $F(q,t)$, according to the relation $F(q,t) \sim \sqrt{\nu(t)}$ that follows from Eq. (8).

component ansatz is the simplest model with the minimum number of free parameters that completely describes the experimental G'' data, which is congruent with our theoretical result derived in the last section, where $\nu(t)$ reduces to a sum of two terms. Surprisingly, we obtain the same fitting parameters for both the experimental and the simulation VDOSs, although the two data sets exhibit noticeably different features. In a way, this result reassures us that the differences in the two VDOSs did not simply "disappear" into the fitting parameters and genuinely implies that these differences do not play a substantial role in the mechanical response. Moreover, it suggests that the qualitative shape of the VDOS, i.e., the location of the peaks, especially on the low-frequency side, is of primary importance. In a broader perspective, this result implies that the origin of the JG β-relaxation in various types of glasses can be traced back to the generic shape of the VDOS and encourages the development of a universal theory based on the microscopic framework employed here.

D. Qualitative behavior of the intermediate-scattering function from theoretical fitting

The square root of $\nu(t)$ is shown in Fig. 4 following the relation $F(q,t) \sim \sqrt{\nu(t)}$ from Eq. (9). We see the characteristic two-step decay of $F(q,t)$ present in systems with well-separated α- and β-relaxations, with the first decay occurring on the typical timescale of the β-relaxation, $\tau_\beta \sim 10^{-7}\ s$, followed by a much slower decay given by the timescale set by τ_1. While the timescale τ_β closely matches the timescale τ_2 set by atomic dynamics dominated by Al, the typical α-relaxation time of glasses, $\tau_\alpha \sim 10^2$ s, is significantly different from the timescale τ_1 associated with Ni, as the α process is more complex, and the square-root mixing of the different timescales of the above relaxation reflects this fact. Moreover, the α peak in G'' and the corresponding decay in $F(q,t)$ cannot be reduced to just τ_1, as the timescale range of the α-relaxation contains a strong contribution from soft modes (the boson peak [29]) in the VDOS. This is clear from Eq. (5), where the term ω_p^2 in the denominator gives a large weight to the low-ω_p part of the VDOS, which contains the BP proliferation of soft modes, as was shown in previous work for the case of CuZr alloys which present only α-relaxation [15] and also for dielectric relaxation of glycerol [16].

VII. CONCLUSION

We have presented a combined experimental, simulation, and theoretical analysis of the viscoelastic response of a metallic glass exhibiting a strong Johari-Goldstein β-relaxation. The appearance of the JG β-relaxation in this metallic glass is attributed to (i) the wide mass disparity between the light Al atoms and the other atomic species and (ii) a strong dynamical coupling involving the Ni and Al atoms at the medium-range order length scale. The results of our theory shed light on the microscopic glassy-state dynamics over a temporal range of 12 orders of magnitude and reproduce the distinctive two-step decay of the intermediate-scattering function that is a characteristic feature of systems exhibiting both β- and α-relaxations. A crucial input to our theory is the vibrational density of states. Surprisingly, only the qualitative features (i.e., peak positions) of the VDOS appear to play the main role in determining the viscoelastic response of the glass, implying a common behavior linking the JG β-relaxation to vibrational dynamics in glassy systems. These results should be useful for developing a universal theory of secondary relaxations in glasses.

ACKNOWLEDGMENTS

We are grateful to the MLZ for the beam time at TOFTOF. B.C. acknowledges the financial support from the CSC-Cambridge Scholarship. P. Luo is gratefully acknowledged for sample preparation.

APPENDIX: DERIVATION OF EQUATION (4)

After taking the Fourier transformation of Eq. (3) in the main text, it becomes

$$-\omega^2 \underline{\tilde{x}}_i + i\tilde{\nu}_i(\omega)\omega \underline{\tilde{x}}_i + \underline{\underline{H}}_{ij}\underline{\tilde{x}}_j = \underline{\Xi}_{i,xy}\tilde{\eta}_{xy}. \tag{A1}$$

Next, we take normal-mode decomposition. This is equivalent to diagonalizing the Hessian matrix $\underline{\underline{H}}$. From now on all matrices and vectors are meant to be $3N \times 3N$ and $3N$-dimensional, respectively. The $3N \times 3N$ matrix $\underline{\underline{H}}$ can be decomposed as $\underline{\underline{H}} = \underline{\underline{\Phi}}\,\underline{\underline{D}}\,\underline{\underline{\Phi}}^{-1} = \underline{\underline{\Phi}}\,\underline{\underline{D}}\,\underline{\underline{\Phi}}^{T}$, where $\underline{\underline{D}}$ is a diagonal matrix filled with the eigenvalues of $\underline{\underline{H}}$, that is, in components, $D_{pp} = \omega_p^2$. Further, the matrix $\underline{\underline{\Phi}}$ consists of the $3N$ eigenvectors $\underline{\phi}_p$ of the Hessian, i.e., $\underline{\underline{\Phi}} = (\underline{\phi}_1, \ldots, \underline{\phi}_p, \ldots, \underline{\phi}_{3N})$, and is an orthogonal matrix.

Then, we left multiply both sides with the matrix $\underline{\underline{\Phi}}^{-1} = \underline{\underline{\Phi}}^{T}$, which leads to Eq. (4) in the main text:

$$-\omega^2(\underline{\underline{\Phi}}^{T}\cdot\underline{\tilde{x}}) + i\omega\underline{\underline{\Phi}}^{T}\underline{\tilde{\nu}}(\omega)\underline{\underline{\Phi}}\,\underline{\underline{\Phi}}^{T}\cdot\underline{\tilde{x}} + \underline{\underline{D}}\,(\underline{\underline{\Phi}}^{T}\cdot\underline{\tilde{x}}) = \underline{\underline{\Phi}}^{T}\cdot\underline{\Xi}_{xy}\tilde{\eta}_{xy},$$

where we used the fact that $\underline{\underline{D}}$ is diagonal and we have dropped all indices i and j and $\underline{\tilde{\nu}}$ is the diagonal matrix $\mathrm{diag}\{\tilde{\nu}_i\}, i = 1, 2, \ldots$.

[1] H. B. Yu, W. H. Wang, H. Y. Bai, and K. Samwer, Natl. Sci. Rev. **1**, 429 (2014).
[2] H. B. Yu, W. H. Wang, and K. Samwer, Mater. Today **16**, 183 (2013).
[3] S. Küchemann and R. Maass, Scr. Mater. **137**, 5 (2017).
[4] G. P. Johari and M. Goldstein, J. Chem. Phys. **53**, 2372 (1970).
[5] K. L. Ngai, J. Non-Cryst. Solids **275**, 7 (2000).
[6] B. Ruta, E. Pineda, and Z. Evenson, J. Phys.: Condens. Matter **29**, 503002 (2017).
[7] M.-T. Cicerone and M. Tyagi, J. Chem. Phys. **146**, 054502 (2017).
[8] Z. G. Zhu, Y. Z. Li, Z. Wang, X. Q. Gao, P. Wen, H. Y. Bai, K. L. Ngai, and W. H. Wang, J. Chem. Phys. **141**, 84506 (2014).
[9] Z. Evenson, S. E. Naleway, S. Wei, O. Gross, J. J. Kruzic, I. Gallino, W. Possart, M. Stommel, and R. Busch, Phys. Rev. B **89**, 174204 (2014).
[10] H.-B. Yu, R. Richert, and K. Samwer, Sci. Adv. **3**, e1701577 (2017).
[11] X. D. Wang, B. Ruta, L. H. Xiong, D. W. Zhang, Y. Chushkin, H. W. Sheng, H. B. Lou, Q. P. Cao, and J. Z. Jiang, Acta Mater. **99**, 290 (2015).
[12] Y. H. Liu, T. Fujita, D. P. B. Aji, M. Matsuura, and M. W. Chen, Nat. Commun. **5**, 3238 (2014).
[13] C. Liu, E. Pineda, D. Crespo, J. Qiao, Z. Evenson, and B. Ruta, J. Non-Cryst. Solids **471**, 322 (2017).
[14] B. Ruta, Y. Chushkin, G. Monaco, L. Cipelletti, E. Pineda, P. Bruna, V. M. Giordano, and M. Gonzalez-Silveira, Phys. Rev. Lett. **109**, 165701 (2012).
[15] B. Cui, J. Yang, J. Qiao, M. Jiang, L. Dai, Y.-J. Wang, and A. Zaccone, Phys. Rev. B **96**, 094203 (2017).
[16] B. Cui, R. Milkus, and A. Zaccone, Phys. Rev. E **95**, 022603 (2017).
[17] A. Meyer, J. Wuttke, W. Petry, A. Peker, R. Bormann, G. Coddens, L. Kranich, O. Randl, and H. Schober, Phys. Rev. B **53**, 12107 (1996).
[18] FRIDA, http://sourceforge.net/projects/frida/.
[19] J. Wuttke, M. Kiebel, E. Bartsch, F. Fujara, W. Petry, and H. Sillescu, Z. Phys. B **91**, 357 (1993).
[20] S. J. Plimpton, J. Comput. Phys. **117**, 1 (1995).
[21] H. W. Sheng, Y. Q. Cheng, P. L. Lee, S. D. Shastri, and E. Ma, Acta Mater. **56**, 6264 (2008).
[22] A. Lemaitre and C. Maloney, J. Stat. Phys. **123**, 415 (2006).
[23] A. Zaccone and E. Scossa-Romano, Phys. Rev. B **83**, 184205 (2011).
[24] R. Milkus and A. Zaccone, Phys. Rev. E **95**, 023001 (2017).
[25] L. Sjoegren and A. Sjoelander, J. Phys. C **12**, 4369 (1979).
[26] B. Bagchi, *Molecular Relaxation in Liquids* (Oxford University Press, Oxford, 2012).
[27] R. Zwanzig, *Nonequilibrium Statistical Mechanics* (Oxford University Press, Oxford, 2002).
[28] J.-P. Hansen and I. R. McDonald, *Theory of Simple Liquids* (Academic, London, 2006).
[29] R. Milkus and A. Zaccone, Phys. Rev. B **93**, 094204 (2016).